

Zero-photon imaging under extremely low-light illumination

De-Zhong Cao,^{1,†,*} Su-Heng Zhang,^{2,†} Yanan Zhao,², Cheng Ren,¹ Jun Zhang,¹ Baolai Liang,² Baoqing Sun,³ and Kaige Wang⁴

¹*School of Opto-Electric Information Science and Technology, Yantai University, Yantai 264005, Shandong Province, China.*

²*College of Physics Science and Technology, Hebei University, Baoding 071002, Hebei Province, China.*

³*School of Information Science and Engineering, Shandong University, Qingdao, 266237, Shandong Province, China*

⁴*Department of Physics, Applied Optics Beijing Area Major Laboratory, Beijing Normal University, Beijing 100875, China.*

[†]These authors contributed equally.

*e-mail address: dzcao@ytu.edu.cn.

Quantum imagers have won accolades for their quantum characteristics¹ and fruitful applications². Ghost imaging exhibited nonlocality with quantum-entangled photons from the parametric down-conversion process³, and later with thermal-light sources^{4,5}. Single-pixel imaging retrieved high-quality images with compressive sensing⁶ and singular valued decomposition⁷ algorithms. Single-photon sensitive apparatus were conducive to first-photon imaging⁸, light-in-flight imaging⁹, photon-efficient imaging¹⁰, and super-remote imaging¹¹. Photon-limited imaging was investigated in low-light-level ghost imaging¹² and fast first-photon ghost imaging^{13,14}. Here in the single-pixel imager scheme, we present zero-photon imaging in which high-quality negative images are reconstructed by correlating the zero-photon measurements and the modulation signals. Also, images are reconstructed with few-photon-state measurements. By comparison, the image quality in ZPI is much higher. This technique may be of significant benefit to rapid pattern recognition and remote sensing.

Quantum imagers greatly exploited the quantum features of the photon detecting devices¹⁵ and the nonclassical light sources^{3,16,17}. Deep information can be discriminated by analyzing the single-photon events registered by quantum detecting devices. Time-correlated single-photon counting (TCSPC) modules were used in microscopic imaging¹⁸ to accurately determine the fluorescence lifetime. Single-photon three-dimension imaging and time-of-flight ranging were carried out by using TCSPC modules and point-by-point acquisition systems¹⁹.

The question that how many photons need to be detected to form an image was unceasingly asked²⁰. Much effort has been made in quantum imaging to pursue the photon-number limit. Remarkably, the photon number necessary involved was greatly decreased in the recent investigations^{12,13,14}, by combining the techniques of computational ghost imaging²¹, and single-pixel compressed sensing^{22,23}. Llull et al.²⁴ analyzed the typical photon numbers for an image and video in compressive temporal imaging. Shin et al. retrieved 3D structure with a single-photon camera in which about one photon detected on each pixel¹⁰. Morris et al. used a small number (about 0.45 photons per pixel) of photons to

implement low-light level imaging¹². Liu et al. achieved images with much smaller photon numbers (about 0.01 photons) per pixel by using fast first-photon ghost imaging (FFGI)¹³ and photon-limited single-pixel imaging¹⁴. Though the photon number may continue to be decreased, this competition will culminate in zero-photon imaging (ZPI).

In this letter, we present ZPI to reconstruct images by correlating zero-photon measurements with modulation signals. We rely on the fact that zero-photon components occupy important positions in the photon-number distribution of the object beam in Fock-state representation. In our experiment, the object beam is extremely attenuated and then is spatially modulated by a digital micromirror device (DMD) with a series of random patterns. A single-photon avalanche detector (SPAD) and TCSPC module are applied to measure the instant photons of the object beam. By just averaging the DMD modulation patterns which are in correspondence to the zero-photon components, we obtain high-quality negative images. By contrast, the image visibility and contrast-to-noise ratio (CNR) in ZPI are prior to that in few-photon measurements, FFGI, and conventional ghost imaging (CGI).

The experimental setup of ZPI is sketched out in Fig. 1a.

The optical source is a super continuum pulsed laser (SCPL) of wavelength 660 nm, frequency 6.49MHz. Before projected onto DMD, the laser beam is expanded by the beam expander (BE), and then is greatly attenuated by a neutral density filter (NDF). The attenuated object beam is registered by a single-pixel SPAD with the help of a collecting lens L. DMD encodes a series of random binary patterns into the pulsed

laser beam. The synchronized pulsed signals from SCPL and SPAD are analyzed by TCSPC module to measure the photon-number distribution of the object beam (See methods). The images are reconstructed by averaging the DMD modulations on condition of zero-photon measurements in the personal computer PC.

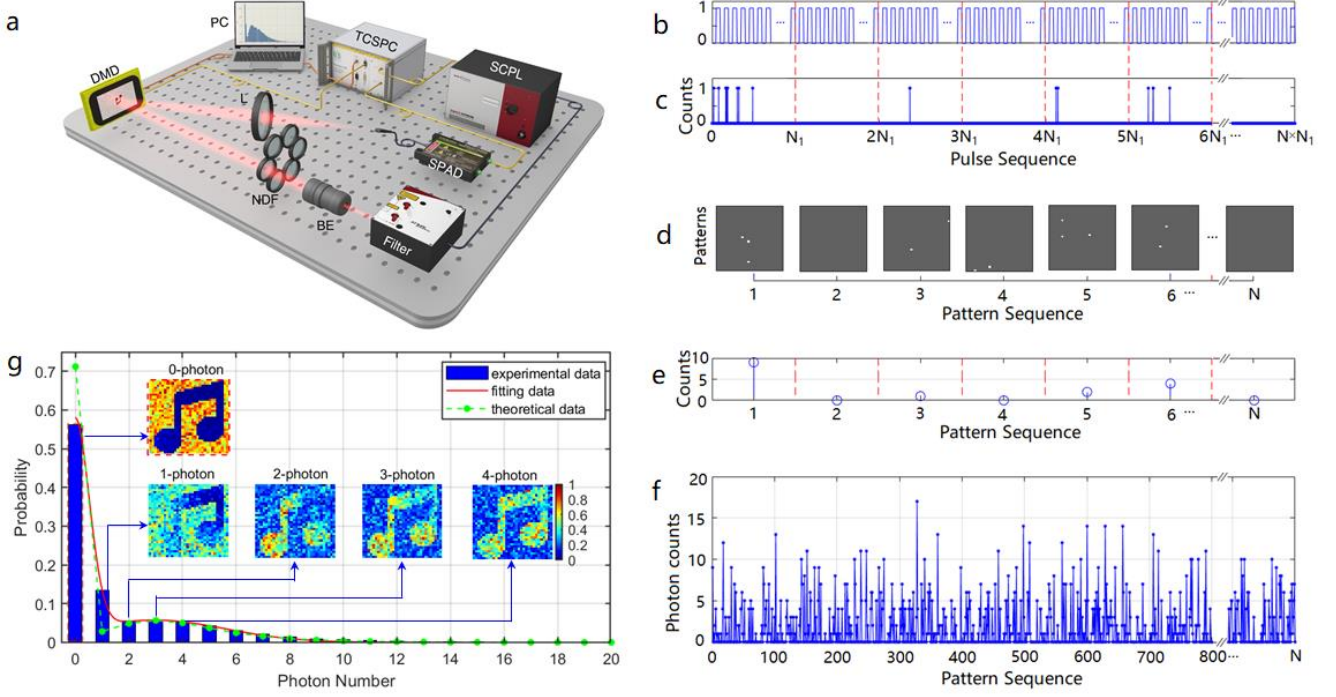


Fig. 1. **a** Schematic of the experimental setup. SCPL represents the super continuum pulsed laser. Filter is used to single out the laser beam of 660nm. BE is the beam expander. NDF is the neutral density filter. DMD is the digital micromirror device. L is the collecting lens. SPAD is the single-photon avalanche detector. TCSPC is the module of time-correlated single-photon counting. PC is the personal computer. **b** Schematic diagram of the $N \times N_1 \approx 2.13 \times 10^9$ pulses which drive SCPL. Here $N = 81,920$ and $N_1 = 25,960$. **c** Photon events detected by SPAD and TCSPC. **d** Independent DMD patterns. **e** Cumulated photon numbers for all the DMD patterns. **f** Exhibition of the first 800 detected signals. **g** photon-number distribution, and reconstructed images Photon-number distribution and reconstructed images.

The pulses driving SCPL are shown in Fig. 1b. Each pulse triggers SPAD, and results in a photon event, 0 or 1, as shown in Fig. 1c. To mimic the photon-number statistics of random sources, the DMD controller loads a set of 81,920 independent binary patterns, as shown in Fig. 1d. Each DMD pattern has 32×32 pixels, and each pixel consists of 8×8 micromirrors. The flipping rate of each DMD pixel is $q = 0.001$. The rate to play these random patterns by DMD is 250 Hz. For each DMD pattern, therefore, 25,960 laser pulses strike the object. The dashed red lines in Figs. 1b and 1c

separate 25,960 pulses and 0/1 photon events in correspondence to each DMD pattern. The cumulated photon events in the DMD pattern interval represent the instant photon number, shown by the blue circles in Fig. 1e. The photon numbers are listed by the blue solid lines with dots in Fig. 1f.

The blue bars in Fig. 1g depicts the histogram of the probability density vs. photon numbers. The averaged photon-number is 1.6. When the photon-number increases from zero, the counting probabilities decline fast, then ascend to the peak

and finally descend slowly to zero. The extraordinary feature is that the zero-photon component, which is surrounded by a dashed red frame, holds a leading position in the photon-number distribution of the object beam. The weight of the zero-photon component is 56.28%. This characterizes the quantum effects of DMD modulation on the photonic mixed states of the object beam.

The mixed state (See Methods) of the photons reflected by each DMD pixel is written as

$$\hat{\rho}_1 = (1-q)|0\rangle\langle 0| + q \sum_{n=0}^{\infty} \frac{\lambda^n}{n!} e^{-\lambda} |n\rangle\langle n|, \quad (1)$$

where the first term is contributed by DMD flipping, the second term fulfills Poisson distribution with photon-number average λ . Accordingly, the multimode mixed state of the object photons registered by SPAD is written by

$\hat{\rho}_M = \sum_{n=0}^{\infty} P_M(n) |n\rangle\langle n|$, where the probability density function (PDF) is

$$P_M(n) = (1-q)^M \delta_n + \sum_{m=1}^M C_M^m q^m (1-q)^{M-m} \frac{(m\lambda)^n}{n!} e^{-m\lambda}, \quad (2)$$

where M is the number of nonzero pixels of the object,

$C_M^m = \frac{M!}{m!(M-m)!}$, and $\delta_n = \begin{cases} 1 & n=0 \\ 0 & n \neq 0 \end{cases}$. The photon-number averages of the single-mode (1) and multimode (2) mixed states are $\bar{n} = q\lambda$ and $Mq\lambda$ respectively.

The zero-photon component occupies an important position for small q . The dashed green line in Fig. 1g is the theoretical curve by Eq. (2), the solid red line is the fitting curve (See Methods).

A virtual object of a music note, which contains 394 nonzero pixels, is pre-mounted onto DMD. The reconstructed image from ZPI is shown in the red dashed box in the subplot in Fig. 1g. A negative image of the music note emerges. The image visibility is $V = 0.93$, and the (peak) CNR^{25} is $R = 5.07$ ($R_p = 25.81$).

Also, the reconstructed images, by averaging the corresponding DMD modulation signals on conditions of 1-photon, 2-photon, 3-photon, and 4-photon measurements, are listed in the subplots of Fig. 1g. With the increase of photon number measured, the retrieved images turn from negative to positive. The quality factors (V , R and R_p) are shown in Fig. 4. We can see that the image quality in ZPI is much higher than others.

The detected photon numbers are in connection with the

DMD modulations (see Methods). In the case that the object value is 1, the joint PDF between the photon-number n of SPAD and DMD pixel value u can be written by

$$P^{(2)}(n,u) = \begin{cases} (1-q)P_{M-1}(n), & (u=0) \\ q \sum_{n_1=0}^n P_{M-1}(n-n_1) \frac{\lambda^{n_1}}{n_1!} e^{-\lambda}. & (u=1) \end{cases} \quad (3)$$

The ZPI image can be obtained by $G_1 = \langle 0|u|0\rangle = P^{(2)}(0,1)$,

that is $G_1 = qe^{-\lambda}(1-q+qe^{-\lambda})^{M-1}$. In the case that the object value is 0, the joint PDF between n and u is given by $P^{(2)}(n,u) = P_M(n)q^u(1-q)^{1-u}$. Accordingly, the image is obtained by $G_0 = q(1-q+qe^{-\lambda})^M$. Since G_1 and G_0 respectively correspond to object value 1 and 0, G_0 represents the background of the reconstructed image.

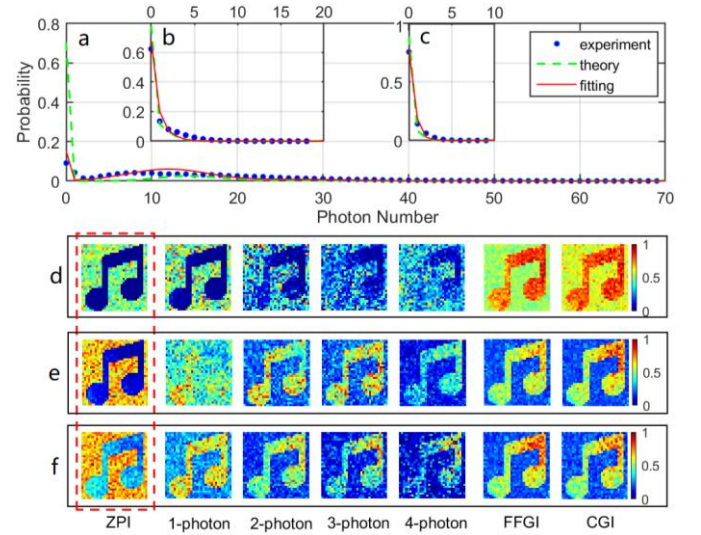


Fig. 2. Photon-number distributions and reconstructed images for photon-number average $\bar{n} = 14.8$ in **a** and **d**, $\bar{n} = 1.0$ in **b** and **e**, and $\bar{n} = 0.4$ in **c** and **f**, respectively. The images from ZPI in the first column are boxed out by the dashed red line. Other images are retrieved from 1-, 2-, 3-, 4-photon measurements and from FFGI and CGI.

Figures 2a, 2b, and 2c show the photon-number probability distributions of object beams with averages $\bar{n} = 14.8$, 1.0 , and 0.4 , respectively. The experimental data are indicated by blue dots. The dashed green and solid red lines are the theoretical and fitting lines. The probability distribution with greater photon-number average has a wider range. No matter what the photon-number average is, the predominance of the zero-photon component is still obvious. The reconstructed

images from ZPI, FFGI, CGI and that from 1-photon, 2-photon, 3-photon, and 4-photon measurements are shown in Figs 2d, 2e, and 2f, which correspond to $\bar{n} = 14.8$, 1.0, and 0.4, respectively. We can see that the ZPI image distinguishes from all the other images by the image quality factors, which are shown in Figs. 4.

To further demonstrate ZPI in Fig. 3a, two real objects, Chinese characters “zhen” (真) and “kong” (空), are employed. The object is projected onto DMD by lens L1. The covered area in DMD has 40×40 pixels. We adopt 40,000 DMD modulation patterns in experiment. All the other experimental parameters are the same as that in Fig. 1a.

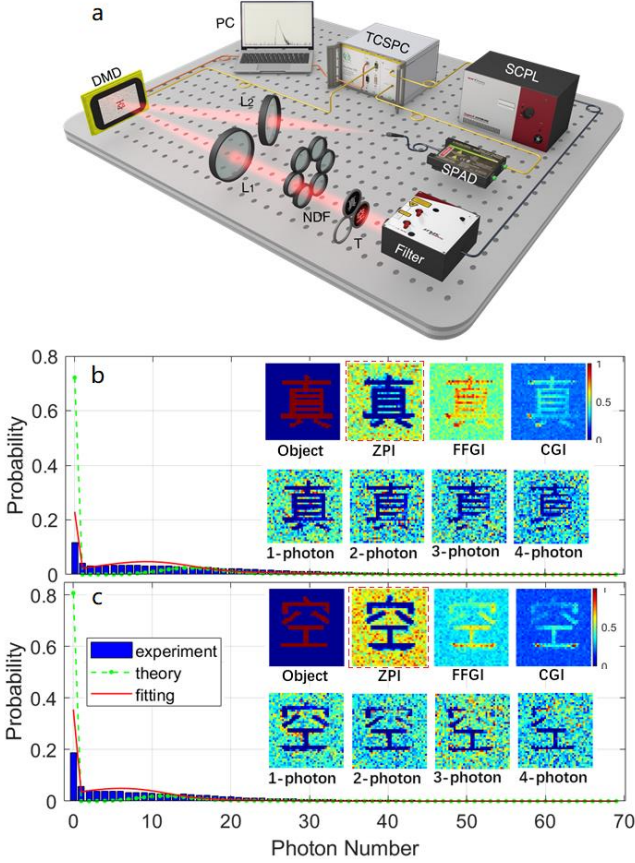


Fig. 3. Image comparison of ZPI, FFGI, and CGI. **a** The photon-number distributions of the object beam from “zhen” and “kong”. **b** The object, ZPI-image, FFGI-image and CGI-image of “zhen”. **c** The object, ZPI-image, FFGI-image and CGI-image of “kong”. All the images are normalized by their maxima.

In Figs. 3b and 3c, the solid blue bars show the photon-number distributions of the object beams from objects “zhen”

and “kong”, respectively. The dashed green lines with dots and the red solid lines are the theoretical and fitting lines. In the two probability distributions for “zhen” and “kong”, the photon-number averages of the object beams are $\bar{n} = 15.4$ and 12.0, respectively. Especially, the proportions of the zero-photon components are 11.73% and 18.77%, which are much greater than that of other photon-number components. We again find the leading positions of the zero-photon components in the two photon-number distributions.

The object of the character “zhen”, which has 363 nonzero pixels, and the reconstructed images from ZPI, FFGI, and CGI, and that from 1-photon to 4-photon measurements are shown in the subplot of Fig. 3b. In the same way, the results of the character “kong”, which has 238 nonzero units, are shown in the subplot of Fig. 3c. The images from ZPI are boxed out by dashed red lines.

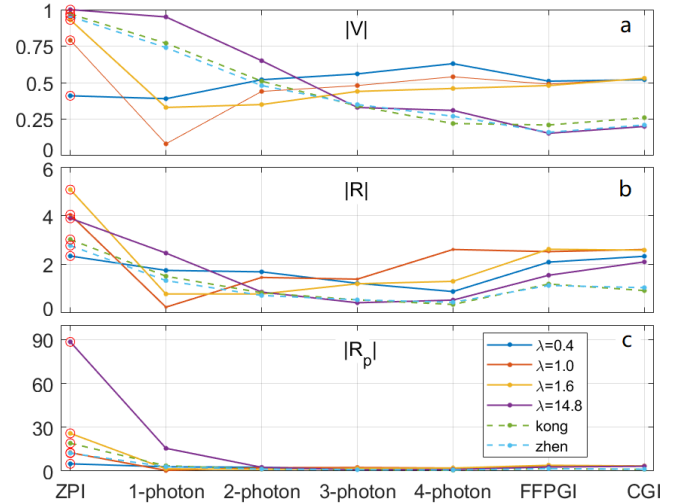


Fig. 4. Quantum Factors of the reconstructed images. a The absolute visibility. **b** The absolute CNR. **c** The absolute peak-CNR.

The quality factors, including the absolute visibility $|V|$, CNR $|R|$, and peak CNR $|R_p|$, of the all the reconstructed images are plotted in Fig. 4. We can see that almost all the factors of images in ZPI are much better than all that in others. The only exception is the visibility in the case of $\bar{n} = 0.4$.

ZPI suggests that the smallest detected photon number for optical imaging reach its bottom of zero. The high quality images make ZPI distinct from ghost imaging and single-pixel imaging scenarios with fast-first-photon

measurements¹³, high-order correlation²⁶, background-subtraction²⁷. Though zero photons are detected, we note that ZPI still consumes a fair number of photons to form the image.

The consumed photon number is proportional to the background area and averaged photon numbers.

References

1. Moreau P. A., Toninelli E., Gregory T. & Padgett M. J. Imaging with quantum states of light. *Nat. Rev. Phys.* **1**, 367–380 (2019).
2. Genovese M. Real applications of quantum imaging. *J. Opt.* **18**, 073002 (2016).
3. Pittman T. B., Shih Y. H., Strekalov D. V. & Sergienko A. V. Optical imaging by means of two-photon quantum entanglement. *Phys. Rev. A* **52**, R3429 (1995).
4. Bennink R. S., Bentley S. J. & Boyd R. W. “Two-Photon” coincidence imaging with a classical source. *Phys. Rev. Lett.* **89**, 113601 (2002).
5. Bennink R. S., Bentley S. J., Boyd R. W. & Howell J. C. Quantum and classical coincidence imaging. *Phys. Rev. Lett.* **92**, 033601 (2004).
6. Duarte M. F., Davenport M. A., Takhar D., Laska J. N., Sun T., Kelly K. F. & Baraniuk R. G. Single-pixel imaging via compressive sampling. *IEEE Signal Process. Mag.* **25**, 83-91(2008).
7. Zhang C., Guo S., Cao J., Guan J. & Gao F. Object reconstitution using pseudo-inverse for ghost imaging. *Opt. Express* **22**, 30063 (2014).
8. Kirmani A., Venkatraman D., Shin D., Colaço A., Wong F. N. C., Shapiro J. H. & Goyal V. K. First-photon imaging. *Science* **343**, 58–61 (2014).
9. Garipey G., Krstajić N., Henderson R., Li C., Thomson R. R., Buller G. S., Heshmat B., Raskar R., Leach J. & Faccio D. Single-photon sensitive light-in-flight imaging. *Nat. Commun.* **6**, 6021 (2015).
10. Shin D., Xu F., Venkatraman D., Lussana R., Villa F., Zappa F., Goyal V. K., Wong F. N. C. & Shapiro J. H. Photon-efficient imaging with a single -photon camera. *Nat. Commun.* **7**, 12046 (2016).
11. Li Z. P., Ye J. T., Huang X., Jiang P. Y., Cao Y., Hong Y., Yu C., Zhang J., Zhang Q., Peng C. Z., Xu F. & Pan J. W. Single-photon imaging over 200 km. *Optica* **8**, 344 (2021).
12. Morris P. A., Aspden R. S., Bell J. E.C., Boyd R. W. & Padgett M. J. Imaging with a small number of photons. *Nat. Commun.* **6**, 5913 (2015).
13. Liu X., Shi J., Wu X. & Zeng G. Fast first-photon ghost imaging. *Sci. Rep.* **8**, 5012 (2018).
14. Liu X., Shi J., Sun L., Li Y., Fan J. & Zeng G. Photon-limited single-pixel imaging. *Opt. Express* **28**, 8132-8144 (2020).
15. Mandel L., Sudarshan E. C. G. & Wolf E. Theory of photo-electric detection of light fluctuations. *Proc. Phys. Soc.* **84**, 435-444 (1964).
16. Treps N., Andersen U., Buchler B., Lam P. K., Maitre A., Bachor H. A. & Fabre C. Surpassing the standard quantum limit for optical imaging using nonclassical multimode light. *Phys. Rev. Lett.* **88**, 203601 (2002).
17. Lemos G. B., Borish V., Cole G. D., Ramelow S., Lapkiewicz R. & Zeilinger A. Quantum imaging with undetected photons. *Nature* **512**, 409–412 (2014).
18. Becker W., Bergmann A., Hink M. A., König K., Benndorf K. & Biskup C. Fluorescence lifetime imaging by time-correlated single-photon counting. *Microsc. Res. Technol.* **63**, 58–66(2003).
19. Buller G. S. & Wallace A. M. Ranging and three-dimensional imaging using time-correlated single-photon counting and point-by-point acquisition. *IEEE J. Sel. Top. Quantum Electron.* **13**, 1006-1015 (2007).
20. Johnson S. D., Moreau P. A., Gregory T. & Padgett M. J. How many photons does it take to form an image? *Appl. Phys. Lett.* **116**, 260504 (2020).
21. Shapiro J. H. Computational ghost imaging. *Phys. Rev. A* **78**, 061802 (2008).
22. Donoho D. L. Compressed sensing. *IEEE Trans. Inf. Theory* **52**, 1289-1306 (2006).
23. Katz O., Bromberg Y. & Silberberg Y. Compressive ghost imaging. *Appl. Phys. Lett.* **95**, 131110 (2009).
24. Llull P., Liao X., Yuan X., Yang J., Kittle D., Carin L., Sapiro G. & Brady D. J. Coded aperture compressive temporal imaging. *Opt. Expr.* **21**, 10526-10545 (2013).
25. Chan K. W. C., O'Sullivan M. N. & Boyd R. W. High-order thermal ghost imaging, *Opt. Lett.* **34**, 3343-3345 (2009).
26. Cao D. Z., Xiong J., Zhang S. H., Lin L. F., Gao L. &

Wang K. Enhancing visibility and resolution in Nth-order intensity correlation of thermal light. *Appl. Phys. Lett.* **92**, 201102 (2008).

27. Chan K. W. C., O'Sullivan M. N. & Boyd R. W.

Methods

Zero-photon measurement. In experiment in Fig. 1a, the pulsed beams, of frequency 6.49MHz and temporal pulse width 20 picoseconds, comes from SCPL (NKT: SuperK EXTREME), and then are greatly attenuated by NDF (Daheng GCC-3010). DMD (ViALUX STAR-07 V7000) contains 1024×768 independently addressable micromirrors, and is used to load random patterns and the virtual music note. The object photons are registered by SPAD (Excelitas SPCM-AQRH-W6) and TCSPC module (PicoQuant PicoHarp 300). The time resolving of TCSPC module is 4 picoseconds.

To clearly count the photons for each DMD pattern, 25,960 laser pulses strike the object. Due to the faint laser, most of the photon events registered by SPAD and TCSPC are zero, as shown in Fig. 1c. The instant photon number for each DMD pattern is obtained by summing the 25,960 photon events, as shown in Fig. 1e. The photon numbers of the first 800 DMD patterns are illustrated by the blue solid lines with dots. In the presented data, the maximum of the photon number is 17, and the minimum is zero. Since each photon number is the sum of sufficient 0/1 events, zero-photon measurement is reliable.

ZPI theory. The randomness of the DMD pixel fulfills Bernoulli distribution $B(u) = q^u(1-q)^{1-u}$, where binary values $u=1,0$ represent the direction of the micromirror forward or backward to SPAD, respectively. The input laser beam is assumed in a coherent state $|\psi\rangle = \sum_{m=0}^{\infty} \frac{\alpha^m}{\sqrt{m!}} e^{-|\alpha|^2/2} |m\rangle$

with photon number average $\lambda = |\alpha|^2$. For $u=1$, the output

beam from the pixel is in the coherent state. But for $u=0$, the output beam is in vacuum state $|0\rangle$. Consequently, the complete state of the output beam is written as the form in Eq. (1). Since the DMD pixels are independent to each other, the photons from each DMD unit can be regarded as in the independent mode as described by Eq. (1). The SPAD signals represent the summed photons from definite DMD pixels. Due to mode-independence, the collected photons by SPAD are in the M -mode mixed state in (2).

The values of u of one DMD pixel obviously affect the

Optimization of thermal ghost imaging: high-order correlations vs. background subtraction. *Opt. Express* **18**, 5562-5573 (2010).

collected object photons. For a definite pixel, the output photons to SPAD are independent to the photons from other $M-1$ units. We assume there are n photons strike SPAD, and n_1 photons are contributed by the definite unit. It is evident that $n-n_1$ photons are from other $M-1$ units. If $u=1$, the PDF of the photon-number n is

$$P'(n) = \sum_{n_1=0}^n P_1(n_1)P_{M-1}(n-n_1) = \sum_{n_1=0}^n P_{M-1}(n-n_1) \frac{\lambda_1^{n_1}}{n_1!} e^{-\lambda_1}. \quad (4)$$

Similarly if $u=0$, all the photons are come from other $M-1$ units, and the PDF of the photon-number n is

$$P''(n) = P_{M-1}(n). \quad (5)$$

By combining Bernoulli distribution of u , PDFs (3) and (4), we arrive at the joint PDF in (3).

The image values are

$$G_1 = qe^{-\lambda}(1-q+qe^{-\lambda})^{M-1}, \quad G_0 = q(1-q+qe^{-\lambda})^M \quad (6)$$

for the respective object values 1 and 0. Consequently, the image visibility is

$$V = \frac{G_1 - G_0}{G_1 + G_0} = \frac{(1-e^{-\lambda})(q-1)}{1-q+qe^{-\lambda}+e^{-\lambda}}. \quad (7)$$

Negative images are obtained since $V < 0$. The fluctuation of the image in ZPI is $\Delta G = \langle u^2 \rangle - \langle u \rangle^2$, and we immediately find

$$\Delta G_1 = G_1 - G_1^2, \quad \Delta G_0 = G_0 - G_0^2. \quad (8)$$

The noise in ZPI can be represented by the above image fluctuations, and we investigate CNR and pCNR²⁵ by

$$R = \frac{G_1 - G_0}{\sqrt{\Delta G_1 + \Delta G_0}}, \quad \text{and} \quad R_p = \frac{G_1 - G_0}{\sqrt{\Delta G_1}}, \quad (9)$$

respectively.

Image visibility, CNR, and pCNR. The quality factors of all the images reconstructed in this letter follow the definitions in (7), (8), and (9), and are shown in Fig. 4. In specific calculations, G_1 and G_0 are the averages of the image pixels in accordance with the object values 1 and 0, so do the fluctuations ΔG_1 and ΔG_0 .

Data fitting of the photon-number distributions. The PDF in Eq. (2) has two features, the unique zero-photon component and incoherent superposition of coherent states. The photon-number distributions measured in experiment deviate from

the theoretical PDF in Eq. (2) to certain extent. We compensate the mismatch by two steps. The first step is to convolve the ideal PDF in with a vector $\vec{l}=[l_1, l_2, l_3]$. The second step is Gaussian fitting. For example, the photon-

Acknowledgments

This research was funded by the National Natural Science Foundation of China (NSFC) (Grant No. 11204062, 11674273) and the Natural Science Foundation of Hebei province (F2019201446).

number PDF becomes

$$P'_M(n)=l_1 \times P_M(n-1)+l_2 \times P_M(n)+l_3 \times P_M(n+1), \quad (10)$$

where $l_1=l_3=1/6.6$, $l_2=5.6/6.6$ are set in Fig. 1g.

Author contributions

D.Z.C. conceived the research and wrote parts of the paper. S.H.Z. constructed zero-photon measuring apparatus, Y.N.Z. did the image reconstruction. S.H.Z and Y.N.Z plotted all the figures. C.R. and B.S. did the numerical simulations and data analyzing, J.Z. and B.L.L. did the data acquisition and extraction, K.W. did the theoretical computation and data fitting. All authors contributed to manuscript preparing and writing. The authors declare no competing interests.